

A Synchronized Reprojection-based Model for 3D Human Pose Estimation

Yicheng Deng¹ · Cheng Sun² · Yongqi Sun^{1*} · Jiahui Zhu¹

Received: date / Accepted: date

Abstract 3D human pose estimation is still a challenging problem despite the large amount of work that has been done in this field. Generally, most methods directly use neural networks and ignore certain constraints (e.g., reprojection constraints and joint angle and bone length constraints). This paper proposes a weakly supervised GAN-based model for 3D human pose estimation that considers 3D information along with 2D information simultaneously, in which a reprojection network is employed to learn the mapping of the distribution from 3D poses to 2D poses. In particular, we train the reprojection network and the generative adversarial network synchronously. Furthermore, inspired by the typical kinematic chain space (KCS) matrix, we propose a weighted KCS matrix, which is added into the discriminator's input to impose joint angle and bone length constraints. The experimental results on Human3.6M show that our method outperforms state-of-the-art methods by approximately 5.1%.

Keywords Human pose estimation · reprojection network · generative adversarial network · kinematic chain space

1 Introduction

3D human pose estimation from monocular images has always been a problem in computer vision. It can

Yicheng Deng · Yongqi Sun · Jiahui Zhu

¹School of Computer and Information Technology, Beijing Jiaotong University, Beijing 100044, P. R. China

E-mail: yqsun@bjtu.edu.cn

Cheng Sun

²School of Information Science and Electrical Engineering, Kyushu University, Fukuoka 8190395, Japan

E-mail: sun.cheng.736@s.kyushu-u.ac.jp

be applied in multiple fields, such as motion recognition, virtual reality, and human-computer interaction. Over the past three decades, there has been a dramatic increase in the field of 3D human pose estimation. Various methods can be divided into two main categories. One category first obtains the 2D joint coordinates from an image[4][5][6][24][26][29][31] and then estimates the 3D pose according to the 2D joint coordinates [15][16][20][33]. The other directly processes the image and estimates the 3D pose through a deep learning method. This paper focuses on the second stage of the first category, which estimates the 3D coordinates of a human pose from the 2D joint coordinates[8][11][17][22][23][35].

Although these methods have achieved good performance, they often ignore the fact that a well-estimated 3D pose should be able to be reprojected back to a plausible 2D pose. Wandt et al.[33] first proposed a model named RepNet to consider the reprojection loss, however, RepNet needs to estimate the camera parameters with deep learning methods, and the training process is somewhat complicated. This paper proposes a weakly-supervised adversarial training method to estimate a 3D human pose. Considering the reprojection constraints and the limitations on bone lengths and joint angles, our estimation results are more accurate and interpretable.

In our method, we employ a generative adversarial network (GAN) to learn the distribution of 3D human poses. First, we set up a generator to generate the depth (the z -component of the 3D coordinates) with the input 2D joint coordinates. Synchronously, we construct a discriminator, whose part of the input is a real 3D pose or a 3D pose generated by the generator, to determine whether the input is from real distribution. Then, we add a network, which does not require extra information such as camera parameters, to reproject the 3D poses

generated by the generator. And we use the reprojection network’s output as our discriminator’s second part of input. Finally, we transform the 3D pose to the weighted kinematic chain space and make it the discriminator’s third part of the input to impose constraints on bone lengths and joint angles. We test our method on three public datasets: Human3.6M[14], MPI-INF-3DHP[21], and MPII[1]. The results of our method outperform those of state-of-the-art methods. Our contributions are as follows:

- We propose an adversarial training structure, which contains a reprojection network without camera parameter requirements, for 3D human pose estimation by simultaneously utilizing the 2D and 3D information.
- We train the generator, the reprojection network and the discriminator synchronously to learn the mapping of the distribution from 2D poses to 3D poses and the inverse mapping.
- We propose an elaborate improved kinematic chain space that transforms a 3D pose into a weighted kinematic chain space to impose constraints on bone lengths and joint angles.

2 Related work

At present, due to large-scale datasets for supervised training and powerful deep neural networks, significant progress has been made in 3D human pose estimation from a monocular image. We can summarize the estimation methods into two categories: end-to-end methods and two-stage methods. The end-to-end methods estimate the 3D joint point position directly from a monocular image and compare it with the 3D annotation to optimize the network. The two-stage methods divide the pose estimation into two stages. The first stage performs 2D pose detection on a single image and predicts its 2D joint coordinates; the second stage predicts 3D joint coordinates from the 2D joint coordinates through regression analysis or model fitting. In this paper, we focus on the second stage of the two-stage methods.

From another perspective, we can further classify 3D estimation methods into three classes: fully supervised methods, unsupervised methods, and weakly supervised methods. In recent years, the GAN proposed by Goodfellow et al.[10] has been a major hit in deep learning, and its application in 3D human pose estimation is also quite extensive.

2.1 Fully supervised methods

There have been several fully supervised 3D estimation methods that make full use of both 2D and 3D ground truths. These fully supervised methods aim to learn the relationship between 2D and 3D data with the help of given paired 2D and 3D data.

Sun et al.[30] propose an end-to-end integral regression model to extract 3D poses from 2D heat maps. Madadi et al.[19] use CNN-based 3D joint predictions as an intermediate representation to regress SMPL pose and shape parameters, and then reconstruct 3D joints in the SMPL output. Dushyant et al. [22] propose a method utilizing a fully CNN, which regresses 2D and 3D joint positions and motion skeleton to produce a real-time stable 3D reconstruction of motion. Different from the end-to-end methods, Martinez et al.[20] use a simple but effective regression network to learn the correspondences from 2D poses to 3D poses without using any image information. Moreno-Noguer[23] implements an approach to learn the correspondence between the 2D distance matrix and 3D distance matrix with a regression model. Wang et al.[34] use 3D data to train an intermediate ranking network and estimate 3D poses from 2D poses by predicting the depth rankings of human joints.

2.2 Unsupervised methods

Unlike supervised methods, unsupervised 3D estimation methods do not involve the 3D ground truth during the training process.

Rhodin et al.[27] propose an encoder-decoder to estimate 3D poses based on unsupervised geometry-aware representations. It requires multiple 2D projections to apply a multiview consistency constraint to learn the appearance representation. Yasunori Kudo et al.[16] design a GAN whose generator uses the x and y coordinates of important joint points as input, and outputs the predicted value of the z -direction component. They assume that if the predicted 3D human body is correct, the 2D reprojection should not collapse even if the 3D human body is rotated at any angle around the y -axis and then projected onto the x - z plane. Chen et al.[7] also design an unsupervised GAN to estimate 3D poses; half of their model is based on a similar strategy and reprojects the generator’s output 3D estimation back to the 2D reprojection, which is used as the input of the discriminator. The other half of their model lifts the 2D reprojection to a 3D pose again and reprojects this 3D pose back to 2D once more.

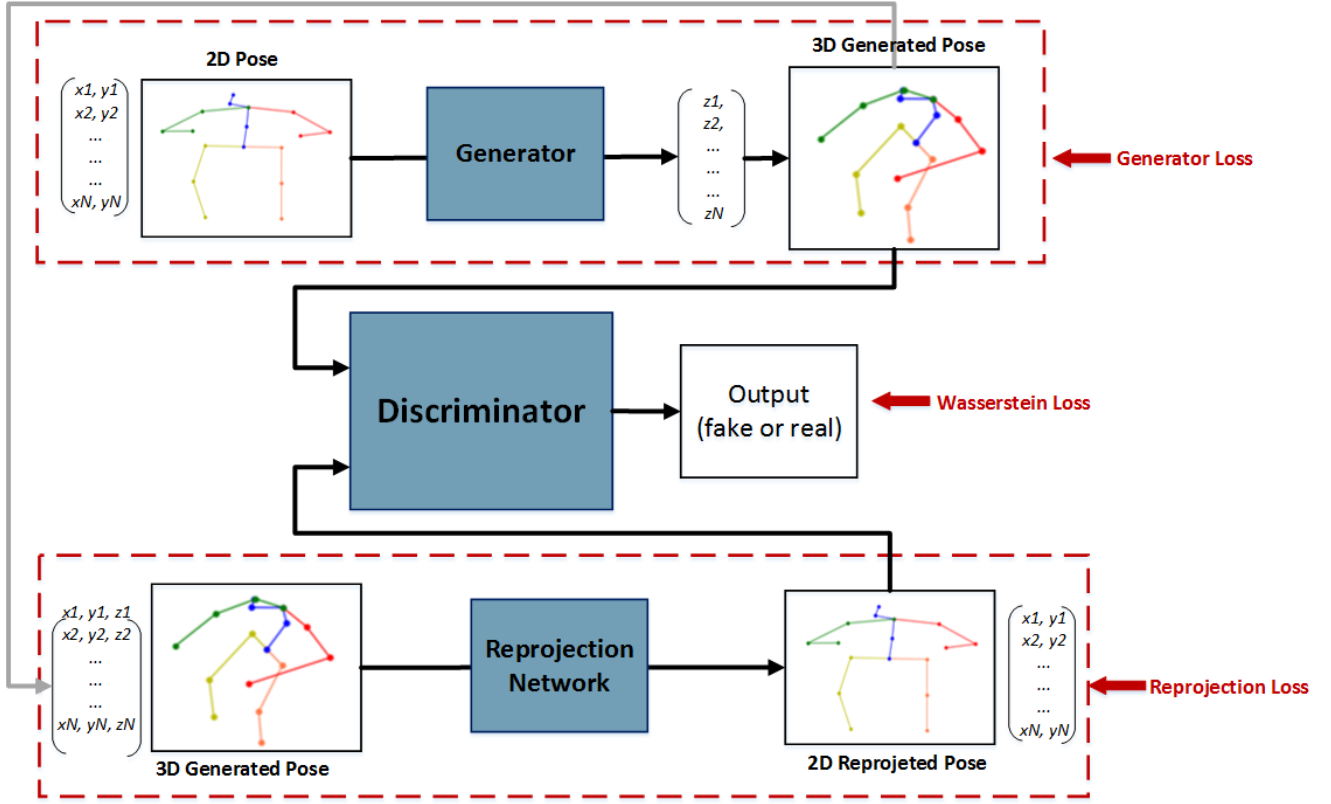


Fig. 1 The main structure of our proposed adversarial training framework, which contains 4 parts: (1) generator, (2) discriminator, (3) reprojection network, and (4) three loss functions. Our structure takes 2D reprojected poses and 3D generated poses into consideration simultaneously. In practice, the generator, discriminator and reprojection network will be trained synchronously.

2.3 Weakly supervised methods

Weak supervision only requires limited 3D labels or an unpaired 2D-3D correspondence. Zhou et al.[38] propose a two-stage transfer model to generate 2D heat maps and regress the joint depths to estimate 3D poses. The 2D and 3D data are mixed during the training process. Hsiao-Yu Fish Tung et al.[32] propose an adversarial inverse graph network model. This model uses the presentation feedback of the prediction results to map the image to the latent factors and matches the distribution between the predicted results and the ground truth latent factors.

Recently some weakly supervised methods have been proposed based on adversarial architectures and reprojection constraints, that is, an estimated 3D pose should be correctly projected back to the 2D pose. Yang et al.[35] implement an adversarial architecture based on multiple representations, including RGB images, geometric representations and heat maps to estimate 3D poses from in-the-wild 2D images. Bastian Wandt et al.[33] propose a GAN-based model named RepNet to learn a mapping from a distribution of 2D poses to a

distribution of 3D poses with an adversarial training approach, in which a camera estimation network is a part of the generator.

In summary, most recent unsupervised and weakly supervised methods involving adversarial structures only consider the consistency constraints between 2D poses and 2D reprojections or among several lifted 3D poses[7]. In this paper, we propose a weakly supervised method that considers 3D estimations along with 2D reprojections simultaneously and train a reprojection network with a GAN synchronously. We also propose a weighted KCS matrix and use it as one part of the discriminator's input to improve the 3D pose estimation accuracy. The experimental results show that our model outperforms state-of-the-art methods.

3 Methods

For a given 2D pose, our goal is to estimate its corresponding 3D pose. The framework we use can be formulated as a GAN. In standard GAN training, the generator's input is a Gaussian distribution or a uniform

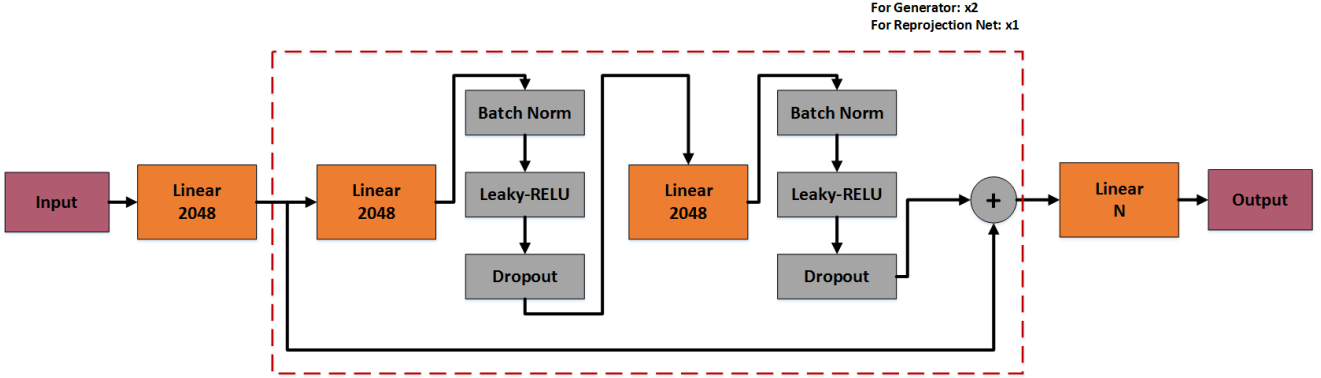


Fig. 2 The structure of our generator and re-projection network is roughly the same as Martinez[20]. The generator has two residual blocks, and the re-projection network has only one residual block. The generator’s input is a 2D pose, and the output is the corresponding z -direction component. In contrast, the re-projection network’s input is a 3D pose, and the output is the related re-projected 2D pose.

distribution. The discriminator is used to determine whether the input data are from the real distribution or generated by the generator. The generator and discriminator are trained alternately. Finally, alternate training makes the generator’s output increasingly closer to the distribution of the real data.

Unlike a standard GAN, in our network architecture, the generator’s input is sampled from a distribution of 2D joint locations in human poses (including the x and y coordinates) obtained from the RGB images. The generator generates reasonable z -components of the 3D human poses without the camera parameters. However, due to its randomness, it is highly probable that the generated 3D pose is far from the real 3D pose. Hence, we employ more constraints to improve the generator’s performance to produce a more realistic 3D pose. Our network architecture is shown in Figure 1.

3.1 Generator

The input of our generator is 2D joint coordinates $X_{real} \in \mathbb{R}^{2N}$, where N represents the number of joints. The generator’s output $Z \in \mathbb{R}^N$ represents the z -components corresponding to the 2D input, and then, we can obtain the corresponding 3D poses $Y_{pred} \in \mathbb{R}^{3N}$. The neural network input is written as a $2N$ -dimensional vector, and the output is an N -dimensional vector. Our generator is designed to learn the mapping from a 2D distribution to a 3D distribution. Its network architecture is shown in Figure 2 and is similar to Martinez’s architecture[20], which has two residual blocks[12], each of which contains two hidden layers, batch norms[13], Leaky-RELU[2], dropout[28], etc.

3.2 Reprojection net

To produce a more realistic 3D pose, we impose re-projection constraints on it; that is, the generator’s 3D pose can still be re-projected back to the original 2D pose. Our re-projection network’s input is the generated 3D pose $Y_{pred} \in \mathbb{R}^{3N}$, and the output is the re-projected 2D pose $X_{rep} \in \mathbb{R}^{2N}$. Instead of training it alone, we use the generated 3D pose together with the re-projected 2D pose as two parts of the discriminator’s input and train the three networks synchronously so that our re-projection net can learn the mapping from the distribution of 3D poses to 2D poses instead of a simple correspondence. In this way, our re-projection net can provide more reliable weakly supervised information to train the generator. Through many experiments, we find that the result of this synchronous training strategy is better than the result obtained by training the re-projection network alone. The structure of our re-projection network is shown in Figure 2. It is similar to the structure of our generator but only includes one residual block.

3.3 Discriminator

Our discriminator network architecture is shown in Figure 3, and its input has three parts: the 3D pose, 2D pose, and weighted KCS matrix. The 3D pose part is the generated or the ground truth 3D poses, and the 2D pose part is the re-projected or ground truth 2D locations. In the following, we describe the weighted KCS matrix.

Inspired by the work of Wandt et al.[33], we design a novel matrix for the bone lengths and joint angles based on the kinematic chain space (KCS) matrix.

Unlike the original KCS, we adopt a weighted KCS by considering each bone’s angle information with any

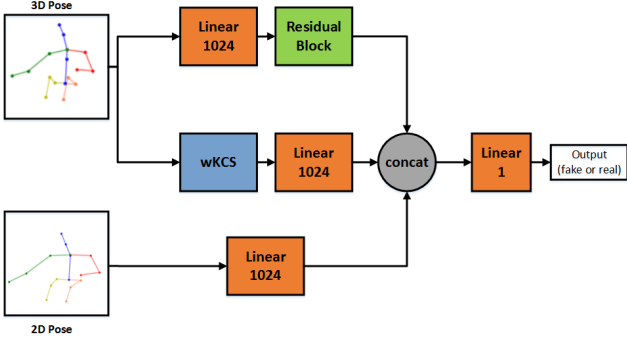


Fig. 3 The structure of the discriminator.

other bone. The main idea is that for the human pose estimation, the closer the distance between two bones, the more critical their angle information. In practice, we transform the 3D human poses into a weighted KCS and make it one part of discriminator's input.

In the following, we describe the calculation method for the weighted KCS matrix. First, similar to[33], we define a piece of bone b_k as the vector between the r -th joint and the t -th joint,

$$b_k = p_r - p_t = Yc, \quad (1)$$

where

$$c = (0, \dots, 0, 1, 0, \dots, 0, -1, 0, \dots, 0)^T. \quad (2)$$

c has j terms, and the terms 1 and -1 represent the start and end indexes of a bone vector, respectively. Let $C \in \mathbb{R}^{j \times b}$ contain the start and end indexes of all bones, where b represents a 3D pose with b bones. Hence, we have

$$B = (b_1, b_2, \dots, b_b) = YC, \quad (3)$$

and we obtain the following KCS matrix:

$$KCS = B^T B. \quad (4)$$

Next, we determine the weight w_{ij} of each element of the KCS. We define a bone distance d_{ij} to represent the distance between the i -th bone and the j -th bone. For example, as shown in Figure 4, we give the bone distances from the right hip bone, where the distance to itself is defined to be 0. There are three bones whose distances are 1, and two bones whose distances are 5. By the bone distances of each bone to any other bone, the weight w_{ij} of the KCS matrix is calculated as follows:

$$w_{ij} = \begin{cases} 1, & i = j \\ 1, & d_{ij} = 1 \\ \tanh\left(\frac{1}{(d_{ij}-1)}\right), & d_{ij} > 1 \end{cases} \quad (5)$$

In the definition, for the matrix's diagonal elements, i.e., $i = j$, we keep the bone length information without the

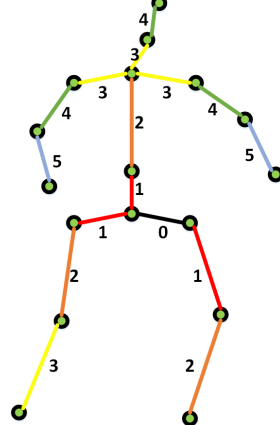


Fig. 4 The bone distances d_{ij} from the right hip bone.

weights. For each bone's adjacent bones, i.e., $d_{ij} = 1$, their knowledge of the joint angles did not change. Let $W \in \mathbb{R}^{b \times b}$ contain all the items of w_{ij} ; then, we obtain the following weighted KCS matrix:

$$wKCS = W * KCS. \quad (6)$$

In practice, the weighted KCS matrix is easy to calculate. Since the wKCS contains information on bone lengths and joint angles, it is more convenient for optimizing the generator to obtain a more proper 3D human pose.

Back to our discriminator's input, the 3D pose part can create a feature vector through a fully connected layer and a residual block, the 2D pose part generates a feature vector through a fully connected layer, and the weighted KCS part also generates a feature vector through a fully connected layer. The three feature vectors have the same dimension. They are then concatenated and fed into a fully connected layer, which generates the discriminator's output. Let

$$p_{real} = D^*(Y_{real}, X_{real}, wKCS_{real}), \quad (7)$$

$$p_{fake} = D^*(Y_{pred}, X_{rep}, wKCS_{pred}), \quad (8)$$

where $wKCS_{pred}$ represents the weighted KCS matrix of the generated 3D pose, and $wKCS_{real}$ represents the weighted KCS matrix of the ground-truth 3D pose. p_{real} is the discriminator's output when the ground truth 3D poses and the ground truth 2D locations are fed to the discriminator and p_{fake} is the discriminator's output when the generated 3D poses and the reprojected 2D locations are the input.

3.4 Loss functions

First, for the GAN, we use the Wasserstein loss function[18], i.e.,

$$L_{dis} = p_{fake} - p_{real}. \quad (9)$$

To train our three networks synchronously, the loss function of the generator is the same as that of the reprojection network,

$$L_{gen} = L_{rep} = -p_{fake}. \quad (10)$$

Then, we impose another constraint L_{angle} , which guarantees that the z -components of the generated 3D pose will not be inverted, by referring to Yasunori[16]. Similarly, we define the face orientation vector $v = [v_x, v_y, v_z] = j_{nose} - j_{neck} \in \mathbb{R}^3$ and shoulder orientation vector $w = [w_x, w_y, w_z] = j_{ls} - j_{rs} \in \mathbb{R}^3$, where $j_{nose}, j_{neck}, j_{ls}, j_{rs} \in \mathbb{R}^3$ represent the 3D coordinates of the nose, neck, left shoulder and right shoulder respectively. According to the above mentioned constraints, the angle β between v and w on the $z - x$ plane should satisfy

$$\sin \beta = \frac{v_z w_x - v_x w_z}{\|v\| \|w\|} \geq 0. \quad (11)$$

To satisfy this inequality, let

$$L_{angle} = \max(0, -\sin \beta) = \max(0, \frac{v_x w_z - v_z w_x}{\|v\| \|w\|}). \quad (12)$$

Finally, through equations (10) and (12), we obtain the final loss function of the generator as follows:

$$L_{gen} = -p_{fake} + \lambda L_{angle}, \quad (13)$$

where λ represent the weight coefficients of the loss terms L_{angle} , respectively.

3.5 Data processing

We performed data preprocessing on the data before training. Like most pose estimation methods, we use the human hip joint as the root joint and subtract the coordinates of the other joint points from the root joint by translating them relative to the root node. Then, we divide the value of all joint coordinates by the corresponding ratio, which is the average of the Euclidean distances from all joints to the root joint. In the training and testing phases, we use these coordinates to represent each joint's position.

3.6 Training details

As mentioned above, we use the standard Wasserstein GAN (WGAN) loss function and our loss function L_{angle} to train our generator, reprojection network, and discriminator synchronously during each iteration. We use the Adam optimizer for all three networks with a learning rate of 8e-5, $\text{beta}_1 = 0.0$ and $\text{beta}_2 = 0.9$. The loss weights are set as $\lambda = 1$.

4 Experiments

Dataset We perform experiments on the three datasets, Human3.6M[14], MPI-INF-3DHP[21] and MPII[1]. Human3.6M is the most popular benchmark dataset for 3D human pose estimation and contains over 3.6 million 3D human poses and the corresponding images. To compare our results with the results of the state-of-the-art methods in related fields, we also use the 2D locations estimated by the stacked hourglass[24] method on the Human3.6M[14] dataset to perform 3D estimation experiments. Finally, we test our model on the MPII dataset, and the experimental results show that our model performs well, even on the dataset whose images are captured from a monocular camera.

4.1 Quantitative evaluation on Human3.6M

Protocols For the Human3.6M dataset, we use S1, S5, S6, S7, and S8 as the training sets and S9 and S11 as the testing sets. The evaluation standard is the mean per joint positioning error (MPJPE). The MPJPE calculates the average Euclidean distance between the estimated 3D pose and the ground truth 3D pose. In the experiments, there are two main protocols to follow: protocol #1 calculates the MPJPE directly and protocol #2 calculates the MPJPE after aligning the estimation with the ground truth via a rigid transformation[3][23].

Results under protocol #1 The experimental results obtained following protocol #1 are shown in Table 1, where the effects of 3D pose estimation, marked as GT, are obtained using ground truth 2D locations for both training and testing. It is shown that our model can obtain stable and balanced pose estimations, and the results outperform the best comparison results by approximately 5.1%.

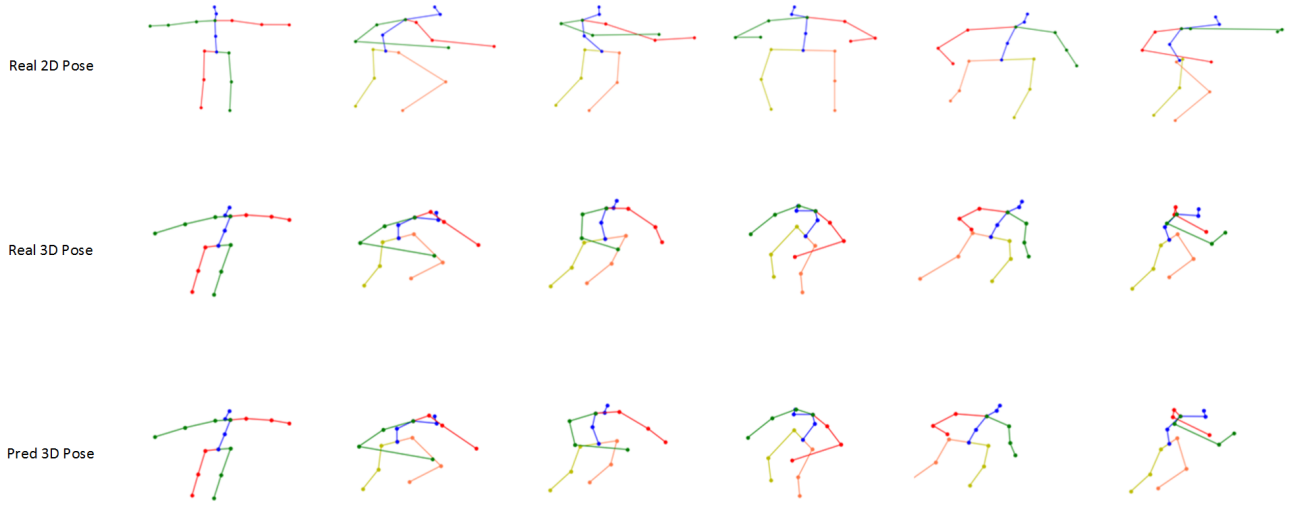
The results, marked as SH-SH, are obtained from 2D locations detected by stacked hourglass for training and testing. We can find that the average MPJPE is 102.2 mm. This error contains two parts: one is from the z -component estimated by our generator, and the other is from the $x-y$ component detected by stacked hourglass instead of our model.

To evaluate the error of the z -component estimated by our generator, we use the 2D locations detected by stacked hourglass for training and testing but only calculate the error of the z -component of the 3D pose, marked as SH-SH-z in Table 1.

To evaluate the model more precisely, we implement the SH-GT experiment. Its training set is the 2D locations detected by stacked hourglass, and the testing set is the ground truth 2D locations. The results of

Table 1 The results of 3D human pose estimation of the Human3.6M dataset compared to other state-of-the-art methods following Protocol #1, all referred results come from the related papers.

Protocol #1	GT	Direct	Discuss	Eating	Greet	Phone	Photo	Pose	Purch	Sitting	SittingD	Smoke	Wait	WalkD	Walk	WalkT	Avg
LinKDE[14]		132.7	183.6	132.3	164.4	162.1	205.9	150.6	171.3	151.6	243.0	162.1	170.7	177.1	96.6	127.9	162.1
Du et al.[8]		85.1	112.7	104.9	122.1	139.1	135.9	105.9	166.2	117.5	226.9	120.0	117.7	137.4	99.3	106.5	126.5
Zhou et al.[37]		87.4	109.3	87.1	103.2	116.2	143.3	106.9	99.8	124.5	199.2	107.4	118.1	114.2	79.4	97.7	113.0
Tang et al.[32]	✓	53.7	71.5	82.3	58.6	86.9	98.4	57.6	104.2	100.0	112.5	83.3	68.9	-	57.0	-	79.0
Martinez et al.[20]		53.3	60.8	62.9	62.7	86.4	82.4	57.8	58.7	81.9	99.8	69.1	63.9	50.9	67.1	54.8	67.5
Kudo et al.[16]		125.0	137.9	107.2	130.8	115.1	127.3	147.7	128.7	134.7	139.8	114.5	147.1	130.8	125.6	151.1	130.9
Zhou et al.[38]	✓	54.8	60.7	58.2	71.4	62.0	65.5	53.8	55.6	75.2	111.6	64.1	66.0	63.2	51.4	55.3	64.9
Yang et al.[35]		51.5	58.9	50.4	57.1	62.1	65.4	49.8	52.7	69.2	85.2	57.4	58.4	60.1	43.6	47.7	58.6
Pavlakos et al.[25]		67.4	71.9	66.7	69.1	72.0	77.0	65.0	68.3	83.7	96.5	71.7	65.8	74.9	59.1	63.2	71.9
B.Wandt et al.[33]	✓	50.0	53.5	44.7	51.6	49.0	58.7	48.8	51.3	51.1	66.0	46.6	50.6	42.5	38.8	60.4	50.9
Ours (GT)	✓	43.3	52.9	42.5	48.7	45.9	59.8	44.9	45.9	49.5	55.9	44.9	49.6	51.3	43.0	45.9	48.3
Ours (SH-SH)		93.7	102.7	95.8	103.8	117.9	113.7	93.7	103.1	111.5	133.6	104.4	99.9	106.5	94.1	97.5	104.8
Ours (SH-GT)		57.9	64.9	60.1	64.4	68.0	74.4	62.5	68.6	67.5	87.3	59.9	65.3	63.1	55.7	61.6	65.4
Ours (SH-SH-z)		43.9	52.6	46.4	53.4	64.9	63.8	48.0	50.5	60.0	84.7	52.5	51.8	56.2	41.7	45.6	54.4

**Fig. 5** Some reconstruction results on the Human3.6M dataset. The first row is ground truth 2D poses, the second row is ground truth 3D poses, and the third row is the reconstructed 3D pose predicted by our model.**Table 2** The results of 3D human pose estimation of the Human3.6M dataset compared with other state-of-the-art methods following Protocol #2, all referred results come from the related papers.

Protocol #2	GT	Direct	Discuss	Eating	Greet	Phone	Photo	Pose	Purch	Sitting	SittingD	Smoke	Wait	WalkD	Walk	WalkT	Avg
Zhou et al.[36]		99.7	95.8	87.9	116.8	108.3	107.3	93.5	95.3	109.1	137.5	106.0	102.2	110.4	106.5	115.2	106.7
Sun et al.[30]	✓	36.9	36.2	40.6	40.4	41.9	34.9	35.7	50.1	59.4	40.4	44.9	39.0	30.8	39.8	36.7	40.6
Bogo et al.[3]		62.0	60.2	67.8	76.5	92.1	77.0	73.0	75.3	100.3	137.3	83.4	77.3	79.7	86.8	87.7	82.3
Martinez et al.[20]		39.5	43.2	46.4	47.0	51.0	56.0	41.4	40.6	56.5	69.4	49.2	45.0	49.5	38.0	43.1	47.7
Fang et al.[9]		38.2	41.7	43.7	44.9	48.5	55.3	40.2	38.2	54.5	64.4	47.2	44.3	47.3	36.7	41.7	45.7
B.Wandt et al.[33]	✓	33.6	38.8	32.6	37.5	36.0	44.1	37.8	34.9	39.2	52.0	37.5	39.8	34.1	40.3	34.9	38.2
Ours (GT)	✓	32.1	36.6	30.1	36.3	31.4	39.6	33.4	31.4	34.5	40.8	33.5	34.8	36.1	30.9	34.7	34.4
Ours (SH-SH)		70.8	75.2	73.4	78.2	88.0	80.1	70.3	71.3	86.3	98.8	82.4	72.3	79.6	74.5	79.1	78.7
Ours (SH-GT)		41.5	43.6	39.9	45.5	46.4	49.9	44.4	44.8	46.5	67.2	44.2	45.0	45.4	39.6	43.9	45.9
Ours (SH-SH-z)		31.6	35.4	31.9	36.8	40.0	39.5	33.5	32.8	41.3	50.3	38.4	34.4	37.8	30.0	33.9	36.5

these experiments show that our model works well for estimating the depth of human poses.

Results under protocol #2 The experimental results under protocol #2, which uses a rigid alignment with the ground truth, are shown in Table 2. We find that our results are better than those of other state-of-the-art methods.

Robustness to detector noise Similar to [23], we add Gaussian noise to the ground truth 2D locations to train and test our model. The mean value of the Gaussian noise is 0, and its standard deviation values are 5, 10, 15, and 20. We perform three groups of experiments as shown in Table 3. The top part includes the results obtained by applying Gaussian noise to training and testing and then calculating the MPJPE. The middle

Table 3 Robustness to detector noise of our model on the Human3.6M dataset following protocol #2.

Protocol #2	test	GT	Error	Direct	Discuss	Eating	Greet	Phone	Photo	Pose	Purch	Sitting	SittingD	Smoke	Wait	WalkD	Walk	WalkT	Avg
GT		MPJPE	32.1	36.6	30.1	36.3	31.4	39.6	33.4	31.4	34.5	40.8	33.5	34.8	36.1	30.9	34.7	34.4	
GT+N(0, 5)		MPJPE	50.7	51.6	48.9	55.1	51.3	57.5	51.8	49.3	51.9	55.7	51.8	51.1	54.4	47.7	51.9	52.1	
GT+N(0, 10)		MPJPE	72.3	73.9	71.6	77.8	74.3	80.0	74.6	73.5	75.4	83.7	75.3	75.7	78.0	73.7	76.1	75.7	
GT+N(0, 15)		MPJPE	96.3	97.1	95.8	100.7	97.1	102.5	96.5	97.1	98.5	106.9	97.5	97.6	101.4	95.8	100.4	98.8	
GT+N(0, 20)		MPJPE	115.7	116.3	119.9	120.9	118.0	125.3	116.5	116.9	120.7	132.0	117.2	120.4	120.6	119.9	121.2	120.1	
GT+N(0, 5)	✓	MPJPE	37.5	38.2	35.6	42.9	38.3	46.4	38.9	34.9	39.5	41.9	38.9	38.1	41.6	33.7	38.5	39.0	
GT+N(0, 10)	✓	MPJPE	42.2	43.1	40.7	48.5	45.4	52.9	45.9	41.2	45.6	53.7	45.2	44.9	47.5	42.9	46.7	45.8	
GT+N(0, 15)	✓	MPJPE	45.9	48.0	46.3	52.1	50.8	58.2	48.8	46.9	51.5	58.5	49.4	48.1	54.6	44.4	52.7	50.4	
GT+N(0, 20)	✓	MPJPE	51.8	50.7	55.1	58.3	53.9	63.1	52.6	49.8	54.5	70.5	51.9	56.9	56.9	57.2	58.9	56.1	
GT+N(0, 5)		only z	30.9	32.8	30.4	35.4	33.9	37.6	34.3	30.6	33.8	36.7	34.1	33.1	35.3	29.1	32.1	33.3	
GT+N(0, 10)		only z	36.3	38.7	36.1	42.2	40.1	44.8	40.6	38.7	40.5	47.9	40.8	41.1	42.7	38.2	40.0	40.6	
GT+N(0, 15)		only z	42.3	43.9	41.7	46.8	45.1	48.8	45.1	44.6	46.0	53.6	45.1	45.6	48.3	42.9	46.6	45.8	
GT+N(0, 20)		only z	43.9	45.3	48.8	49.8	49.0	54.5	44.8	44.9	51.9	63.4	47.4	50.8	49.5	40.0	48.1	49.4	

part contains the results obtained by applying Gaussian noise only to training but testing on ground-truth then calculating the MPJPE. The bottom part includes the results obtained by applying Gaussian noise to training and testing and then calculating the z -component error only. Because our generator estimates only the z component of a 3D pose, the distance between the x - y coordinates increases when we use the noise-applied 2D locations for testing. Therefore, we use the second and third experiments to evaluate our model and to verify its reliability. The experimental results show that our model can still perform well in estimating the human pose depth even if the 2D detector produces noise.

4.2 Quantitative evaluation on MPI-INF-3DHP

We also perform experiments on the MPI-INF-3DHP dataset[21], and the experimental results are shown in Table 4. The higher the PCK value or the lower the MPJPE value is, the better the model performs. The results show that our model has achieved the best 3DPCK and a good ranking for MPJPE among all existing methods. Hence, our model can be applied to multiple datasets and achieves better performance in human pose estimation.

Table 4 The results of 3D human pose estimation on the MPI-INF-3DHP dataset.

Methods	3D PCK	MPJPE
Mehta et al.[21]	76.5	117.6
VNect[22]	76.6	124.7
Zhou et al.[38]	69.2	137.1
OriNet[17]	81.8	89.4
Yang et al.[35]	69.0	-
RepNet[33]	82.5	97.8
Ours	86.0	94.9

Table 5 Ablation studies.

Methods	Human3.6M	MPI-INF-3DHP
	MPJPE	3DPCK / MPJPE
Sep + KCS	50.6	84.4 / 98.9
Sep + wKCS	49.9	84.8 / 98.1
Syn + KCS	49.6	84.5 / 98.2
Syn + wKCS	48.3	86.0 / 94.9

4.3 Ablation studies

In this section, we conduct ablation studies to evaluate the effectiveness of our synchronous training strategy and the weighted KCS. The experimental results on Human3.6M and MPI-INF-3DHP are shown in Table 5, where Sep and Syn represent our separate and synchronous training strategies, respectively.

Sep+wKCS represents our experimental results when we train the GAN and the reprojeciton network separately and use the wKCS as one part of our discriminator's input. We find that the estimation accuracy in such experiments is worse, and the training process is unstable. In contrast, our strategy that trains them synchronously works well; it obtains more accurate and stable pose estimations.

Syn+KCS represents our experimental results when we train our model synchronously and use the common KCS instead of our wKCS. The results show that our wKCS can make the generator concentrate on more critical joint angle information, i.e., the angle information between bones with a smaller bone distance.

4.4 Qualitative evaluation on MPII

We finally conduct experiments on the MPII dataset[1], which has only 2D annotations. The experimental results are shown in Figure 6. It can be seen that our model performs well with a standard 2D pose dataset, which contains more complicated in-the-wild poses.

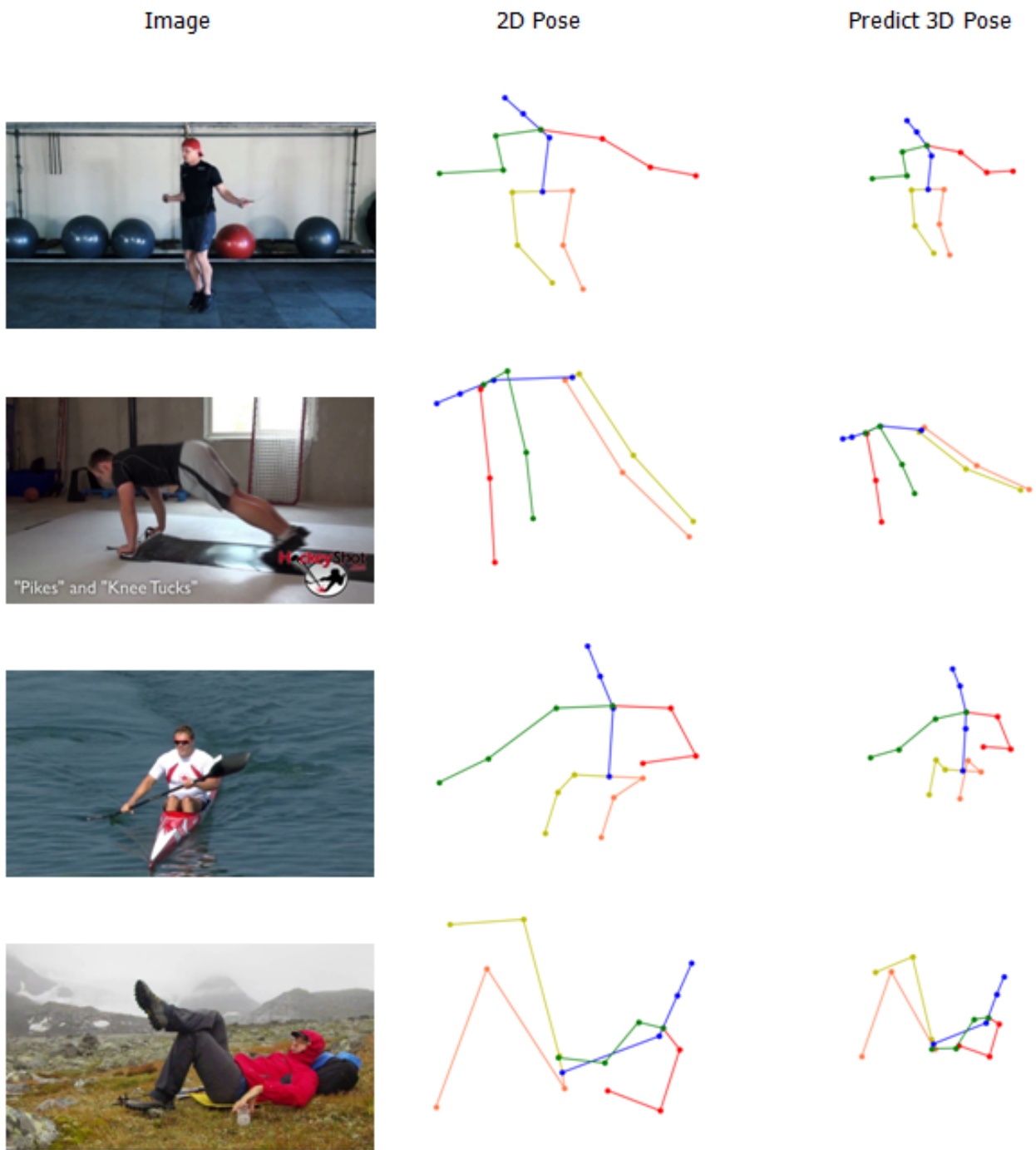


Fig. 6 Some reconstruction results on the MPII dataset. Each of 2D Pose is the ground truth 2D coordinates, and each of Predict 3D Pose is the 3D pose predicted using our model.

5 Conclusion

Many effective models have been developed to estimate 3D human poses. However, most of them only focus on the consistency between 2D poses and 2D reprojections or among several lifted 3D poses to perform this task. This paper proposes a synchronized adversarial architecture that utilizes 2D and 3D information simultaneously to estimate 3D human poses from monocular images. Based on a GAN, we add a reprojection network to learn the mapping of the distribution from 3D human poses to 2D reprojections and synchronously train the reprojection network with the generator as well as the discriminator. We also design a improved space that transforms a 3D pose into a weighted kinematic chain space to impose the constraints on joint angles and bone lengths. The experimental results show that our method outperforms the state-of-the-art methods by approximately 5.1% on Human3.6M and achieves more accurate estimation performance than those methods on MPI-INF-3DHP and MPII. In the future, we plan to improve the model’s performance by applying it to multiview images or videos.

Acknowledgment

This research is supported by the National Natural Science Foundation of China (NSFC 61572005, 61672086, 61702030, 61771058).

References

1. Mykhaylo Andriluka, Leonid Pishchulin, Peter Gehler, and Bernt Schiele. Human pose estimation: New benchmark and state of the art analysis. In *Computer Vision and Pattern Recognition (CVPR)*, 2014.
2. B Xu, N Wang, T Chen, M Li. Empirical evaluation of rectified activations in convolutional network. 2015.
3. Federica Bogo, Angjoo Kanazawa, Christoph Lassner, Peter Gehler, Javier Romero, and Michael J. Black. Keep it smpl: Automatic estimation of 3d human pose and shape from a single image. In *European Conference on Computer Vision*, 2016.
4. Adrian Bulat and Georgios Tzimiropoulos. Human pose estimation via convolutional part heatmap regression. In *European Conference on Computer Vision*, 2016.
5. Zhe Cao, Tomas Simon, Shih En Wei, and Yaser Sheikh. Realtime multi-person 2d pose estimation using part affinity fields. In *2017 IEEE Conference on Computer Vision and Pattern Recognition (CVPR)*, 2017.
6. Joao Carreira, Palkit Agrawal, Katerina Fragkiadaki, and Jitendra Malik. Human Pose Estimation with Iterative Error Feedback. In *2016 IEEE Conference on Computer Vision and Pattern Recognition (CVPR)*, pages 4733–4742, Las Vegas, NV, USA, June 2016. IEEE.
7. Ching Hang Chen, Ambrish Tyagi, Amit Agrawal, Dylan Drover, M. V. Rohith, Stefan Stojanov, and James M. Rehg. Unsupervised 3d pose estimation with geometric self-supervision. In *2019 IEEE/CVF Conference on Computer Vision and Pattern Recognition (CVPR)*, 2020.
8. Yu Du, Yongkang Wong, Yonghao Liu, Feilin Han, and Weidong Geng. Marker-less 3d human motion capture with monocular image sequence and height-maps. In *European Conference on Computer Vision*, 2016.
9. Haoshu Fang, Yuanlu Xu, Wenguan Wang, Xiaobai Liu, and Song Chun Zhu. Learning pose grammar to encode human body configuration for 3d pose estimation. 2017.
10. Goodfellow, I, Pouget-Abadie, J, Mirza, M, Xu, B, Warde-Farley, D, Ozair, S, Courville, A, and Bengio, Y. Generative adversarial nets. 2014.
11. H.-Y. Tung, H.-W. Tung, E. Yumer, and K. Fragkiadaki. Self-supervised learning of motion capture. *Advances in Neural Information Processing Systems 30*, pages 5236–5246. Curran Associates, Inc, 2017.
12. Kaiming He, Xiangyu Zhang, Shaoqing Ren, and Jian Sun. Deep residual learning for image recognition. In *IEEE Conference on Computer Vision and Pattern Recognition*, 2016.
13. Sergey Ioffe and Christian Szegedy. Batch normalization: Accelerating deep network training by reducing internal covariate shift. In *ICML*, 2015.
14. C Ionescu, D Papava, V Olaru, and C Sminchisescu. Human3.6m: Large scale datasets and predictive methods for 3d human sensing in natural environments. *IEEE Transactions on Pattern Analysis and Machine Intelligence*, 36(7):1325–1339, 2014.
15. Yeonho Kim and Daijin Kim. A cnn-based 3d human pose estimation based on projection of depth and ridge data. *Pattern Recognition*, 106:107462, 2020.
16. Yasunori Kudo, Keisuke Ogaki, Yusuke Matsui, and Yuri Odagiri. Unsupervised adversarial learning of 3d human pose from 2d joint locations. 2018.
17. Chenxu Luo, Xiao Chu, and Alan Yuille. Orinet: A fully convolutional network for 3d human pose estimation. In *BMVC*, 2018.
18. M. Arjovsky, S. Chintala, and L. Bottou. Wasserstein generative adversarial networks. In D. Precup and Y. W. Teh, editors, *Proceedings of the 34th International Conference on Machine Learning*, volume 70 of *Proceedings of Machine Learning Research*, pages 214–223, International Convention Centre, Sydney, Australia, 06–11 Aug 2017. PMLR.
19. Meysam Madadi, Hugo Bertiche, and Sergio Escalera. Smplr: Deep learning based smpl reverse for 3d human pose and shape recovery. *Pattern Recognition*, 106:107472, 2020.
20. Julieta Martinez, Rayat Hossain, Javier Romero, and James J. Little. A simple yet effective baseline for 3d human pose estimation. In *2017 IEEE International Conference on Computer Vision (ICCV)*, 2017.
21. Dushyant Mehta, Helge Rhodin, Dan Casas, Pascal Fua, Oleksandr Sotnychenko, Weipeng Xu, and Christian Theobalt. Monocular 3d human pose estimation in the wild using improved cnn supervision. In *3D Vision(3DV)*, 2017.
22. Dushyant Mehta, Srinath Sridhar, Oleksandr Sotnychenko, Helge Rhodin, and Christian Theobalt. Vnect: Real-time 3d human pose estimation with a single rgb camera. *ACM Transactions on Graphics*, 36(4), 2017.
23. Francesc Moreno-Noguer. 3d human pose estimation from a single image via distance matrix regression. In *Computer Vision and Pattern Recognition*, 2017.
24. Alejandro Newell, Kaiyu Yang, and Jia Deng. Stacked hourglass networks for human pose estimation. In *ECCV*, 2016.

25. Georgios Pavlakos, Xiaowei Zhou, Konstantinos G Derpanis, and Kostas Daniilidis. Coarse-to-fine volumetric prediction for single-image 3d human pose. In *IEEE Conference on Computer Vision and Pattern Recognition*, 2017.
26. Leonid Pishchulin, Eldar Insafutdinov, Siyu Tang, Bjoern Andres, Mykhaylo Andriluka, Peter Gehler, and Bernt Schiele. Deepcut: Joint subset partition and labeling for multi person pose estimation. In *Computer Vision and Pattern Recognition*, 2016.
27. Helge Rhodin, Mathieu Salzmann, and Pascal Fua. Unsupervised geometry-aware representation for 3d human pose estimation. In *European Conference on Computer Vision*, 2018.
28. Nitish Srivastava, Geoffrey Hinton, Alex Krizhevsky, Ilya Sutskever, and Ruslan Salakhutdinov. Dropout: A simple way to prevent neural networks from overfitting. *Journal of Machine Learning Research*, 15(1):1929–1958, 2014.
29. Ke Sun, Bin Xiao, Dong Liu, and Jingdong Wang. Deep high-resolution representation learning for human pose estimation. In *2019 IEEE/CVF Conference on Computer Vision and Pattern Recognition (CVPR)*, 2019.
30. Xiao Sun, Bin Xiao, Fangyin Wei, Shuang Liang, and Yichen Wei. Integral Human Pose Regression. In Vittorio Ferrari, Martial Hebert, Cristian Sminchisescu, and Yair Weiss, editors, *Computer Vision – ECCV 2018*, volume 11210, pages 536–553. Springer International Publishing, Cham, 2018. Series Title: Lecture Notes in Computer Science.
31. Alexander Toshev and Christian Szegedy. DeepPose: Human Pose Estimation via Deep Neural Networks. In *2014 IEEE Conference on Computer Vision and Pattern Recognition*, pages 1653–1660, Columbus, OH, USA, June 2014. IEEE.
32. Hsiao Yu Fish Tung, Adam W. Harley, William Seto, and Katerina Fragkiadaki. Adversarial inverse graphics networks: Learning 2d-to-3d lifting and image-to-image translation from unpaired supervision. In *2017 IEEE International Conference on Computer Vision (ICCV)*, 2017.
33. Bastian Wandt and Bodo Rosenhahn. Repnet: Weakly supervised training of an adversarial reprojection network for 3d human pose estimation. *IEEE Conf. Computer Vision and Pattern Recognition (CVPR)*, 2019.
34. Min Wang, Xipeng Chen, Wentao Liu, Chen Qian, Liang Lin, and Lizhuang Ma. Drpose3d: Depth ranking in 3d human pose estimation. In *Proceedings of the Twenty-Seventh International Joint Conference on Artificial Intelligence, IJCAI-18*, pages 978–984. International Joint Conferences on Artificial Intelligence Organization, 7 2018.
35. Wei Yang, Wanli Ouyang, Xiaolong Wang, Jimmy Ren, Hongsheng Li, and Xiaogang Wang. 3D Human Pose Estimation in the Wild by Adversarial Learning. In *2018 IEEE/CVF Conference on Computer Vision and Pattern Recognition*, pages 5255–5264, Salt Lake City, UT, USA, June 2018. IEEE.
36. Xiaowei Zhou, Menglong Zhu, Spyridon Leonardos, and Kostas Daniilidis. Sparse representation for 3d shape estimation: A convex relaxation approach. *IEEE Transactions on Pattern Analysis and Machine Intelligence*, pages 1–1, 2016.
37. Xiaowei Zhou, Menglong Zhu, Spyridon Leonardos, Konstantinos G. Derpanis, and Kostas Daniilidis. Sparseness Meets Deepness: 3D Human Pose Estimation from Monocular Video. In *2016 IEEE Conference on Computer Vision and Pattern Recognition (CVPR)*, pages 4966–4975, Las Vegas, NV, USA, June 2016. IEEE.
38. Xingyi Zhou, Qixing Huang, Xiao Sun, Xiangyang Xue, and Yichen Wei. Towards 3d human pose estimation in the wild: a weakly-supervised approach. In *2017 IEEE International Conference on Computer Vision (ICCV)*, 2017.